Agricultural Water Management 209 (2018) 178–187

Contents lists available at ScienceDirect

Agricultural Water Management

journal homepage: www.elsevier.com/locate/agwat

Simulation of soil water flow and heat transport in drip irrigated potato field with raised beds and full plastic-film mulch in a semiarid area

You-Liang Zhang[a,b], Shao-Yuan Feng[a,b], Feng-Xin Wang[a,*], Andrew Binley[c]

[a] Center for Agricultural Water Research in China, China Agricultural University, No. 17 Qinghua East Road, Haidian, Beijing 100083, China
[b] College of Hydraulic Energy and Power Engineering, Yangzhou University, Yangzhou 225009, China
[c] Lancaster Environment Centre, Lancaster University, Lancaster LA1 4YQ, United Kingdom

ARTICLE INFO

Keywords:
Soil water and heat
Full plastic-film mulch
Surface drip irrigation
Potato
Soil hydraulic parameters
HYDRUS-2D

ABSTRACT

Surface drip irrigation with full plastic-film mulch can increase crop yield and save water by regulating soil water and heat conditions for potato (*Solanum tuberosum* L.) production with raised beds in semiarid area where the rainfall is scarce and evaporation is high. For efficient use of plastic film mulch an understanding of the soil water flow and heat transport is needed. Here we use a model (HYRUS-2D) which is calibrated with field experiments to simulate soil water movement and heat transport. The field experiments were conducted with three treatments, characterized as wetted soil percentages: 35% (P1), 55% (P2), and 75% (P3). Furthermore, the effects of the uncertainty of key soil hydraulic parameters on soil water contents were evaluated using three approaches: (1) soil hydraulic parameters estimated from measured soil textural information (S1); (2) from experimentally measured soil water retention curve (S2); and (3) from inverse modeling (S3). The performance of S2 was the worst in all treatments; the root mean square error (RMSE) was > 0.05 $cm^3 cm^{-3}$. The performance of S3 was the best with RMSE ranged from 0.015 to 0.038 $cm^3 cm^{-3}$ at 10–50 cm soil depth. The simulated soil water in the raised bed decreased quickly after irrigation, maintaining adequate aeration for potato growth, irrespective of the wetted soil percentage. The downward transport of soil water still existed during the second and third days after irrigation in the simulations of the P2 and P3 treatments. The soil temperatures between the P1 and P3 treatments were similar. In conclusion, the HYDRUS-2D simulations could be used to estimate the soil hydraulic and thermal parameters with inverse modeling. The calibrated model can be used in the design and management of surface drip irrigation with raised beds and full plastic-film mulch to provide favorable soil water and heat conditions for potato growth.

1. Introduction

Surface drip irrigation with plastic-film mulching is widely used in agriculture and horticulture. The combination of surface drip irrigation and plastic-film mulching increases water and fertilizer use efficiency and crop yield (Assouline, 2002; Darwish et al., 2003; Tiwari et al., 2003; Phogat et al., 2014). Moreover, plastic-film mulch can modify the radiative and thermal conditions in the fields, which improves plant growth (Liakatas et al., 1986; Wang et al., 2011; Yaghi et al., 2013).

The advantages of this technology depend upon design and management which based on thorough understanding of spatiotemporal distribution of soil water and heat. The main goal is to match the soil wetted volume with root pattern and match soil water storage with crop evapotranspiration (Patel and Rajput, 2008). Many factors can affect the soil wetted volume, such as the soil hydraulic properties, emitter discharge, emitter spacing, wetted soil percentage, etc. The wetted soil percentage is an important parameter used in the design and management of drip irrigation system (Keller and Karmeli, 1974; Zur, 1996). Both soil water and heat stress can affect potato tuber growth, yield, and potato quality (Van Dam et al., 1996; Shock et al., 2007). It is, therefore, important to obtain soil water and heat dynamics in drip irrigated potato field under different wetted soil percentages with raised beds and plastic-film mulch.

Field experiments are costly, time-consuming, and site specific (Subbaiah, 2013). Therefore, analytical and numerical modeling methods are widely used to predict the soil water flow and heat transport and spatial-temporal distribution under various conditions (Coelho and Or, 1997; Cook et al., 2003; Šimůnek et al., 2008). Among these models, the HYDRUS model is popular and useful in simulation of soil water flow, solute, and heat transport (Šimůnek et al., 2008). This

* Corresponding author.
E-mail address: fxinwang@cau.edu.cn (F.-X. Wang).

https://doi.org/10.1016/j.agwat.2018.07.021
Received 28 May 2018; Received in revised form 18 July 2018; Accepted 21 July 2018
Available online 30 July 2018
0378-3774/

model has been used to simulate effects of different soil types and fertigation strategies (Gärdenäs et al., 2005; Hanson et al., 2006), emitter discharges (Ajdary et al., 2007), pulsed and continuous irrigation (Phogat et al., 2012, 2014), bed geometries (Holt et al., 2017), and partial plastic-film mulch (Liu et al., 2013; Chen et al., 2014; Wang et al., 2014; Li et al., 2015a,b; Holt et al., 2017; Qi et al., 2018) on soil water and solute transport under surface drip irrigation. The process of soil water and heat transport has also been simulated in winter wheat field with plastic-film mulch under no irrigation (Zhao et al., 2018). However, the effects of different wetted soil percentages on soil water flow and heat transport have not been evaluated with HYDRUS under surface drip irrigation with raised beds and full plastic-film mulch for potato crops. For potatoes in semiarid area, the raised beds and full plastic-film mulching can retain more soil water in plant root zone (Qi et al., 2018) and produce higher yield and water use efficiency in comparison to partial plastic-film mulch (Zhao et al., 2014).

Soil hydraulic parameters greatly affect the simulation results of soil water transport. Inverse models can be used to estimate soil hydraulic and thermal parameters (Šimůnek and Genuchten, 1996; Hopmans et al., 2002; Mortensen et al., 2006; Nakhaei and Šimůnek, 2014). In this study we validate the applicability of the inverse model with data from potato field. The objectives of this study are to: (1) evaluate the applicability of HDRUS-2D for soil water and heat simulation under drip irrigation with raised beds and full plastic-film mulch; (2) compare simulations of HYDRUS-2D results with soil hydraulic parameters derived from three different approaches (estimated from soil textural information, from experimentally soil water retention curve, and from inverse modeling); and (3) analyze the effects of different wetted soil percentages on soil water and heat transport and spatial-temporal distributions under surface drip irrigation with raised beds and full plastic-film mulch.

2. Materials and methods

2.1. Field experimental site and design

Field experiments were carried out at the Shiyanghe Experimental Station of China Agricultural University, located in Wuwei, Gansu Province (N 37°52′, E 102°50′, altitude 1581 m) from April to August in 2015. This region was characterized by a typical continental temperate climate with mean annual sunshine duration of 3000 h, mean annual temperature 8 °C, and mean annual accumulated temperature (> 0 °C) 3550 °C which was suitable for potato growth. However, agricultural in this region was influenced by scarce water resources with mean annual precipitation of 164 mm, mean annual pan evaporation 2000 mm, and mean groundwater table 25–30 m below land surface.

Potato plants were drip irrigated in raised beds mulched by transparent plastic film and three wetted soil percentages were designed: 35% (P1), 55% (P2), and 75% (P3). Each treatment was replicated three times.

2.2. Agronomic and irrigation practices

The specific descriptions of agronomic and irrigation practices have been presented previously (Zhang et al., 2017a,b). In this manuscript, only main information was included to avoid overlapping. Seed potatoes (30 g, cv. Kexin No.1, Inner Mongolia Minfeng Potato Industry Co., Ltd., Ulanqab, China) were planted every 30 cm in the center of the raised beds at a depth of 15 cm on 15 April 2015. Each plot (6 m × 5.6 m) had 7 north-south raised beds (0.8 m wide and 0.2 m high) which were covered entirely using plastic film mulch (0.008 mm thick, 1.2 m wide). In 2015, 231 kg ha^{-1} P_2O_5 and 90 kg ha^{-1} N were spread before planting and 95 kg ha^{-1} N and 117 kg ha^{-1} K_2O were applied through irrigation after planting.

A drip tape (wall thickness 0.4 mm, inner diameter 16 mm) was placed on the soil surface in the center of each bed. The emitter discharge was 1.38 L h^{-1} at an operating pressure of 0.1 MPa. The drip irrigation system at each plot was managed by a sluice valve, a pressure gauge, a water meter, and a tensiometer. The irrigation application was started when the soil matric potential reached −25 kPa (Wang et al., 2007). The irrigation amount (in mm) was determined using the equation:

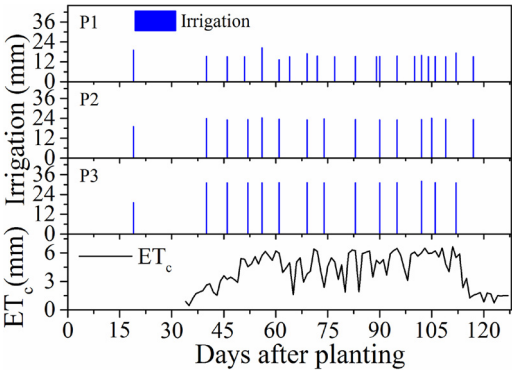

Fig. 1. The amount of each irrigation in 35% soil wetted treatment (P1), 55% soil wetted treatment (P2), and 75% soil wetted treatment (P3). The actual daily evapotranspiration (ET_c) during the growing season.

$$m = h(\theta_a - \theta_b)P/\eta \quad (1)$$

where h is the planned wetted depth (cm) (equal to 50 cm for potato plants), θ_a is the volumetric soil water content after irrigation (cm^3 cm^{-3}) (equal to field capacity 0.27 cm^3 cm^{-3} in this experiment), θ_b is the volumetric water content before irrigation (cm^3 cm^{-3}) (equal to 70% of field capacity), P is the percentage of wetted zone, and η is the coefficient of the efficiency of the drip irrigation system (equal to 0.97 for drip irrigation). The first irrigation amount was 19 mm for all treatments for potato emergence and the subsequent irrigation amount was 15 mm for the P1 treatment, 23 mm for the P2 treatment, and 31 mm for the P3 treatment. The actual irrigation amount used for the P1, P2, and P3 treatments was shown in Fig.1.

2.3. Weather, soil temperature, and soil water content measurements

Meteorological data (precipitation, solar radiation, relative humidity, wind speed, and air temperature) were measured with a standard automatic weather station (HOBO H21-001, Onset Computer Corp., Cape Cod, MA, USA) which was 2 m above the surface of the ground. Before the potato tubers were planted, sensors were installed to measure soil temperature and soil water content. The soil temperatures were measured on the soil surface, and at 5, 10, 20, 30, and 50 cm soil depths both in the middle and at the side (20 cm from the center) of the beds in one replication of each treatment. Soil water contents were measured with sensors at 10, 20, 30, and 50 cm soil depths in the middle, at the side, and at the base (40 cm from the center) of the beds in one replication of each treatment. Sensors on the soil surface and at 5 cm soil depth were thermocouples temperature sensors (ST10, Beijing Unism Technologies, Inc., Beijing, China). Sensors at 10, 20, 30, and 50 cm soil depths in the middle and the side of the beds were soil temperature/water sensors (FDS120, Beijing Unism Technologies, Inc.). Sensors at 10, 20, 30, and 50 cm soil depths in the base of the beds were soil water sensors (FDS100, Beijing Unism Technologies, Inc.). The placement of soil water sensors, temperature sensors, and soil temperature/water sensors was shown in Fig.2. The 10 min average soil temperature and soil water content were recorded automatically with a datalogger (SMC6108, Beijing Unism Technologies, Inc.).

2.4. Hydraulic parameter measurements

Before potato planting, soil samples were taken for soil particle size

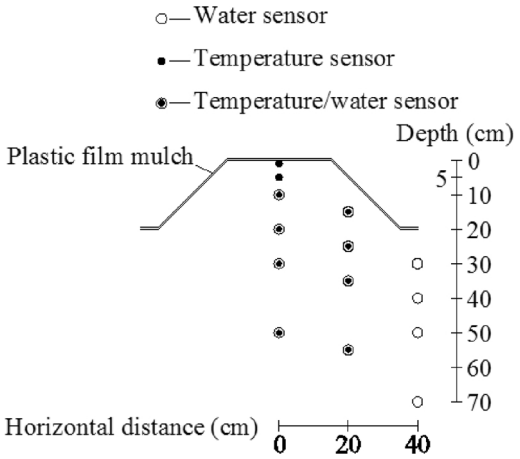

Fig. 2. Placement of soil water sensors, temperature sensors, and soil temperature/water sensors.

analysis using a soil auger in the middle of the beds, down to 10, 20, 30, 50, and 70 cm soil depths in each plot. The soil samples were dried in air and sieved with a 2 mm mesh size. Then, soil particle size was analyzed using a Malvern Mastersizer 2000 laser analyzer (Malvern Instruments Ltd., Malvern, UK) (Ryżak and Bieganowski, 2011). Saturated soil water content (θ_s) and bulk density were measured gravimetrically at 0–20 and 20–40 cm soil depths using a ring sampler (diameter 5 cm, height 5.1 cm, volume 100 cm^3).

After potato harvest, three trenches were dug to take soil samples for soil water retention curve (SWRC) measurements. The undisturbed soil samples (diameter 5 cm, height 5.1 cm, volume 100 cm^3) were taken at 20–40, 40–60, and 60–80 cm soil depths in each trench with three replicates at each layer. Since the shallow soil in the raised beds was disturbed during potato harvest, no soil sample was taken at 0-20 cm soil depth. The soil water retention curve was measured by centrifugation method which has been used widely because of its higher efficiency compared to the ceramic pressure plate method (Šimůnek and Nimmo, 2005; Reatto et al., 2008; Van den Berg et al., 2009; Cropper et al., 2011). The saturated soil samples were centrifuged in a high-speed refrigerated centrifuge (himac CR22GII, Hitachi Koki Co., Ltd., Tokyo, Japan) at different constant rotation speeds (970, 1670, 2160, 2730, 3050, 5290, 6820, 8630, 8830, and 10,800 r/min) in sequences for 60 min (90 min at 8830 and 10,800 r/min) to reach the soil water potential equilibrium. The rotation speeds correspond to different matric potentials (-10, -30, -50, -80, -100, -300, -500, -800, -1000, and −1500 kPa). After each centrifugation, the soil samples were weighed and returned to the centrifuge for another higher rotation speed. When the last centrifugation was finished, soil samples were oven-dried at 105 °C to constant dry weight.

2.5. Model settings

HYDRUS (2D/3D) version 2.05.0200 was applied to simulate soil water and heat transport in the experiments. This code, based on a Galerkin-type linear finite element method, solves Richards' equation for variably-saturated water flow and the advection-dispersion equation for heat and solute transport. The solution also incorporates a sink term in the flow equation to represent root water uptake (Šimůnek et al., 2008, 2016).

2.5.1. Numerical modeling theory for soil water flow

Since the drip emitter distance was small, the soil water flow can be considered as a two-dimensional problem. Without considering the effect of air phase on liquid flow, the flow is governed by the modified Richards' equation:

$$\frac{\partial\theta(h)}{\partial t} = \frac{\partial}{\partial x_i}[K(h)\frac{\partial h}{\partial x_j} + K(h)] - S(h) \quad (2)$$

where θ is the volumetric water content ($cm^3\ cm^{-3}$), h is the pressure head (cm), $K(h)$ is the unsaturated hydraulic conductivity function (cm day^{-1}), x_i and x_j are the spatial coordinates x or z (cm), t is time (day) and $S(h)$ is a sink term denoting root water uptake (day^{-1}). The sink term $S(h)$ is defined according to the model of Feddes et al. (1978). The unsaturated hydraulic conductivity function is given by the van Genuchten-Mualem model (Mualem, 1976; van Genuchten, 1980).

Since the root distribution under drip irrigation is non-uniform, to reflect the spatial variations of root water uptake Vrugt et al. (2001a, 2001b) introduced a two-dimensional dimensionless distribution of root water uptake:

$$\omega(x, z) = (1 - \frac{z}{z_m})(1 - \frac{x}{x_m})e^{-(\frac{p_z}{z_m}|z^*-z| + \frac{p_r}{x_m}|x^*-x|)} \quad (3)$$

where z_m denotes the maximum root depth which is set as 50 cm, x_m denotes the maximum root width which is set as 30 cm, z^* denotes the depth of maximum root intensity which is set as 20 cm, x^* denotes the width of maximum root intensity which is set as 20 cm, and p_z and p_x are empirical parameters which is set as 1.

2.5.2. Numerical modeling theory for heat transport

The two-dimensional heat transport function, ignoring the effects of water vapor, is given by Sophocleous (1979):

$$C(\theta)\frac{\partial T}{\partial t} = \frac{\partial}{\partial x_i}\left[\lambda_{ij}(\theta)\frac{\partial T}{\partial x_j}\right] - C_w q_i \frac{\partial T}{\partial x_i} \quad (4)$$

where $\lambda_{ij}(\theta)$ is the soil apparent thermal conductivity (W $cm^{-1}\ °C^{-1}$), $C(\theta)$ is the total volumetric heat capacity (J $cm^{-3}\ °C^{-1}$), C_w is the volumetric heat capacity of water (J $cm^{-3}\ °C^{-1}$), T is temperature (°C), and q_i is water flux (cm day^{-1}). In addition, the first and second terms on the right side of equation (4) represent heat flow due to conduction and heat transported by flowing water, respectively.

The volumetric heat capacity suggested by de Vries (1963) is as follows:

$$C(\theta) = C_n\theta_n + C_o\theta_o + C_w\theta + C_g a_v \approx (1.92\theta_n + 2.51\theta_o + 4.18\theta)10^6 \quad (5)$$

where the subscripts g, w, o, and n, denote gas phase, liquid phase, organic matter, and solid phase, respectively.

The apparent thermal conductivity $\lambda_{ij}(\theta)$ is described by Šimůnek and Suarez (1993):

$$\lambda_{ij}(\theta) = \lambda_T C_\omega |q|\ \delta_{ij} + (\lambda_L - \lambda_T)C_w\frac{q_j q_i}{|q|} + \lambda_o(\theta)\delta_{ij} \quad (6)$$

where λ_L denotes the longitudinal thermal dispersivity (cm), λ_T denotes the transverse thermal dispersivity (cm), δ_{ij} is the Kronecker delta function, and $\lambda_o(\theta)$ denotes the thermal conductivity. According to Chung and Horton (1987), the $\lambda_o(\theta)$ can be described as follow:

$$\lambda_0(\theta) = b_1 + b_2\theta + b_3\theta^{0.5} \quad (7)$$

where b_1, b_2, and b_3 are empirical parameters (W $cm^{-1}\ °C^{-1}$).

2.5.3. Soil hydraulic functions and thermal parameters

The soil was divided into two layers (0–20 and 20–70 cm soil depths). Three approaches were used to derive the soil hydraulic parameters. Firstly, the Rosetta code (Schaap et al., 2001) in the HYDRUS package was used to estimate the soil hydraulic parameters according to the soil textural distribution and bulk density (Table 1). Secondly, the soil hydraulic parameters at 20–70 cm were estimated from the experimentally measured soil water retention curve (Fig.3) fitted by RETC (van Genuchten et al., 1991), while the parameters at 0–20 cm were the same with the first approach. Thirdly, the soil hydraulic parameters were derived with inverse estimation using a

Table 1
Soil grain size distribution, bulk density, and saturated water content (θ_s) at different depths.

Depth (cm)	Sand (%) 2-0.05 mm	Silt (%) 0.05-0.002 mm	Clay (%) < 0.002 mm	Soil type	Bulk density (g cm^{-3})	θ_s (cm^3 cm^{-3})
0-10	51.2 (5.4[a]) NS	41.4 (4.8[a]) NS	7.4 (0.7[a]) NS	Loam	1.48 (0.05[b])	0.375 (0.009[b])
10-20	51.0 (7.9)	41.6 (6.7)	7.4 (1.6)	Loam		
20-30	52.7 (2.7)	39.9 (2.2)	7.4 (0.5)	Sandy Loam	1.58 (0.06)	0.383 (0.033)
30-50	50.0 (4.4)	42.3 (3.7)	7.7 (0.7)	Loam		
50-70	46.9 (5.8)	45.3 (5.1)	7.8 (0.8)	Loam		

NS: difference among different depths was not significant by F-test ($P > 0.05$).
[a] Values in parentheses denoted the standard deviation with n = 15.
[b] Values in parentheses denoted the standard deviation with n = 9.

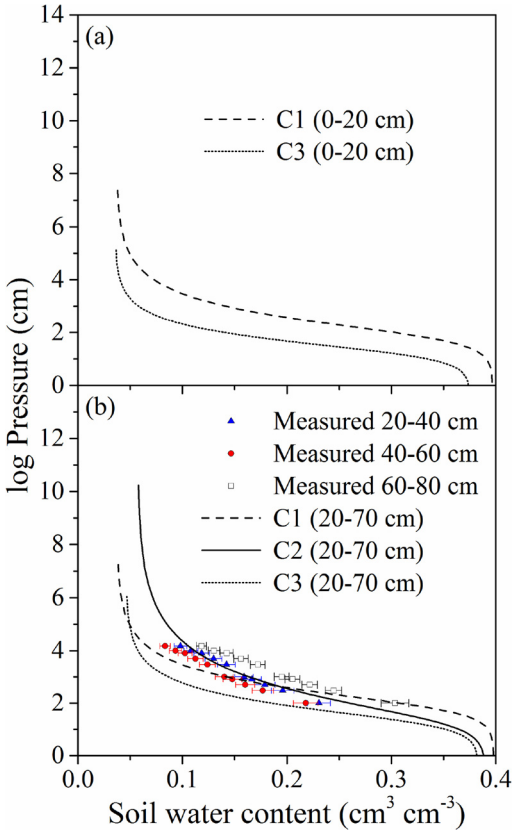

Fig. 3. Soil water retention curves estimated by measured soil textural information (C1), measured experimentally (C2) (measured at 20–40 cm, 40–60 cm, and 60–80 cm soil depths), and estimated by inverse modeling (C3) at: (a) 0–20 cm soil depth; and (b) 20–70 cm soil depth.
Note: Soil water retention curve was not experimentally measured at 0–20 cm soil depth.

Marquardt-Levenberg-type parameter optimization algorithm in HYDRUS-2D. The observed soil water content in the P2 treatment at different soil depths (perpendicular to the drip line at 0, 20 and 40 cm and at increments down to 10, 20, 30, 50 cm) during the whole growing season was used to optimize the soil hydraulic parameters (θ_r, α, n, and K_s). The observed θ_s was used and l was set as 0.5. The soil water retention curves and soil hydraulic parameters obtained with different approaches were shown in Fig.3 and Table 2, respectively.

The thermal parameters b_1, b_2, and b_3 were optimized after the soil hydraulic parameters optimization using the observed soil temperature in the P2 treatment at different soil depths (perpendicular to the drip line at 0 and 20 cm and at increments down to 5, 10, 20, 30, 50 cm) during the whole growing season. The thermal parameters were shown in Table 3.

Table 2
Soil hydraulic parameters (the residual water content θ_r, the saturated water content θ_s, the saturated hydraulic conductivity K_s, and empirical coefficients α, n, and l) estimated from measured soil textural information (S1), from experimentally measured soil water retention curve (S2), and from inverse modeling (S3).

Depth (cm)	θ_r (cm^3 cm^{-3})	θ_s (cm^3 cm^{-3})	α (cm^{-1})	n	K_s (cm day^{-1})	l
S1						
0-20	0.0371	0.397	0.0137	1.471	35.31	0.5
20-70	0.0377	0.398	0.0127	1.485	34.88	0.5
S2						
0-20	0.0371	0.397	0.0137	1.471	35.31	0.5
20-70	0.0517	0.390	0.0508	1.290	34.88	0.5
S3						
0-20	0.0354	0.375	0.0557	1.672	176.90	0.5
20-70	0.0459	0.383	0.0476	1.549	50.72	0.5

2.5.4. Initial and boundary conditions

The wetted region on the vertical plane was assumed to be symmetrical on the left and right sides (Chen et al., 2014) and half of the bed was simulated with the drip emitter being placed at the origin of the coordinates (Fig.4). The initial conditions were the volumetric soil water content and temperature measured at different soil depths on 27 May (DAP 42, one day after irrigation).

A time variable flux was set on one part of the top soil profile (Or′) because of the irrigation. Zero flux was imposed on the other part of the soil surface (r′FED) for water flow because of the plastic-film mulch (Fig.4). Or′ is the soil wetted area during irrigation which was computed by an iterative method (Gärdenäs et al., 2005). It was realized by switching from a Neumann to a Dirichlet boundary condition if the pressure head is larger than zero as the emitter flux was applied (Gärdenäs et al., 2005). Different soil wetted lengths can be obtained for different irrigation fluxes and initial soil water contents. After irrigation, the whole soil surface of the upper boundary condition was imposed as zero flux because of the plastic-film mulch. A free drainage boundary condition was used for the lower boundary condition because of assumed deep ground water. No-flow boundary conditions were prescribed on the left and right sides, assuming that no flow took place along the perpendicular sides. The third type, Cauchy, and the first type, Dirichlet, boundary conditions were used on Or′ and the other part of the top soil profile (r′FED) for heat transport, respectively. No flux boundary conditions were assumed on both sides and third type boundary on the bottom of the profile for heat transport.

2.5.5. Evapotranspiration

The daily crop evapotranspiration (ET_c) was calculated using the dual crop coefficient method and Penman-Monteith equation (Allen et al., 1998):

$$ET_c = (K_{cb} + K_e)ET_o \quad (8)$$

where ET_o is reference crop evapotranspiration calculated according to

Table 3
Soil thermal parameters (the volumetric solid phase fraction θ_n, the volumetric organic matter fraction θ_o, the longitudinal thermal dispersivity λ_L, the transverse thermal dispersivity λ_T, the volumetric heat capacity of solid phase C_n, the volumetric heat capacity of organic matter C_o, the volumetric heat capacity of liquid phase C_w, and empirical parameters b_1, b_2, and b_3) for heat transport simulation.

Depth (cm)	θ_n ($cm^3\,cm^{-3}$)	θ_o ($cm^3\,cm^{-3}$)	λ_L (cm)	λ_T (cm)	b_1 (W cm^{-1} °C^{-1})	b_2 (W cm^{-1} °C^{-1})	b_3 (W cm^{-1} °C^{-1})	C_n (W cm^{-1} °C^{-1})	C_o (W cm^{-1} °C^{-1})	C_w (W cm^{-1} °C^{-1})
0-20	0.66	0	5	1	5.805E+11	2.113E+16	8.975E+16	1.43E+14	1.87E+14	3.12E+14
20-70	0.64	0	5	1	1.385E+16	2.494E+16	9.808E+16	1.43E+14	1.87E+14	3.12E+14

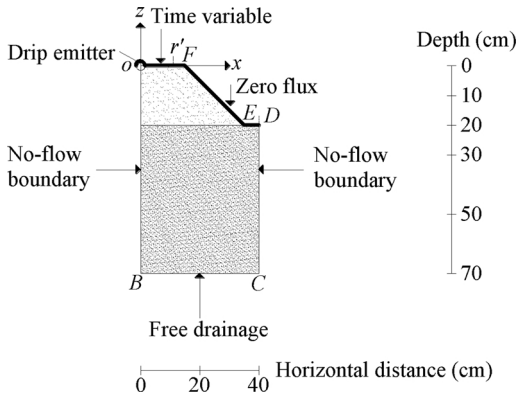

Fig. 4. Scale diagram of the simulated domain and boundary conditions.

the meteorological data, K_{cb} is the basal crop coefficient for crop transpiration, and K_e is the coefficient for soil evaporation. The basal crop coefficient (K_{cb}) used for each growth stage was based on the recommended value by FAO and the actual crop growth. In addition, K_{cb} was 10% larger for crop grown with plastic film mulch than without plastic film mulch according to the guidelines (Allen et al., 1998). The daily transpiration (Fig.1) was used as a time-variable boundary condition. Soil evaporation was neglected because of the full plastic-film mulch.

2.5.6. Model performance

The model efficiency was evaluated by the root mean square errors (*RMSE*), the mean absolute errors (*MAE*), and the mean relative errors (*MRE*):

$$RMSE = \sqrt{\frac{1}{N}\sum_{i=1}^{N}(P_i - O_i)^2} \quad (9)$$

$$MAE = \frac{1}{N}\sum_{i=1}^{N}|P_i - O_i| \quad (10)$$

$$MRE = \frac{1}{N}\sum_{i=1}^{N}\left|\frac{P_i - O_i}{O_i}\right| \quad (11)$$

where N is the number of observations, P_i is the simulated value, and O_i is the observed value.

3. Results and discussion

3.1. Calibration and validation

3.1.1. Soil water content simulation

The model parameters were calibrated with data of the P2 treatment and the model was validated with data of the P1 and P3 treatments. Soil water contents were simulated with soil hydraulic parameters estimated from soil textural information (S1). According to Phogat et al. (2012) the RMSE used to evaluate the satisfaction of soil water content simulation is 0.05 $cm^3\,cm^{-3}$. The performance of S1 for the P1 treatment was not satisfactory because the RMSE of S1 at five positions were larger than 0.05 $cm^3\,cm^{-3}$. The simulated soil water contents of S1 agreed reasonably well with the observed data for the P2 treatment. The RMSE of S1 ranged from 0.014 to 0.039 $cm^3\,cm^{-3}$ with the MRE from 7.1% to 19.9% for the P2 treatment (Table 4). For the P3 treatment the performance of S1 was good for most of the positions with the RMSE ranged from 0.016 to 0.048 $cm^3\,cm^{-3}$ except two positions (10 cm soil depth on the top of the bed and 50 cm soil depth on the base of the bed with the RMSE > 0.05 $cm^3\,cm^{-3}$). The simulated soil water contents of S1 were overestimated at 0–10 cm soil depth on the top and the side of the bed and underestimated at 50 cm soil depth in the base of the bed for the P3 treatment (Fig.5).

Soil water contents were simulated using parameters estimated from measured soil water retention curve (S2). The performance of S2 was not satisfactory for the three treatments because the RMSE at nine positions for the P1 treatment, four positions for the P2 treatment, and ten positions for the P3 treatment were > 0.05 $cm^3\,cm^{-3}$ (Table 4). Dahiya et al. (2007) also reported that the simulation results with experimentally measured soil water retention curve and hydraulic conductivity were not satisfactory.

Soil water contents were simulated with parameters derived from inverse model (S3). The performance of S3 was not satisfactory for the P1 treatment with the RMSE at five positions larger than 0.05 $cm^3\,cm^{-3}$. The RMSE of S3 for the P2 treatment ranged from 0.017 to 0.049 $cm^3\,cm^{-3}$ with the MRE from 6.9% to 20.1%. The simulated soil water contents of S3 at 50 cm soil depth in the base of the bed were underestimated for the P3 treatment and the RMSE was quite large (0.078 $cm^3\,cm^{-3}$). The RMSE of S3 at the other soil depths ranged from 0.015 to 0.038 $cm^3\ cm^{-3}$ for the P3 treatment with the MRE from 6.9% to 20.8%.

Both the S1 and S3 did not have good simulation results for the P1 treatment and at 50 cm soil depth in the base of the bed of the P3 treatment. This might be because the soil properties in these positions were much different to those of the overall soil. The reason for the unsatisfactory simulation of S2 might be caused by the scale effects of the ring sample size (Zhao et al., 2010). Comparing with S3, the performance of S1 was poor at 10 cm soil depth. This might be because the hydraulic conductivity estimated from the soil textural information was smaller than the actual value. Overall, as the inverse model could adjust the soil hydraulic parameters effectively to fit the observed soil water contents, the performance of S3 was the best.

3.1.2. Soil heat simulation

Generally, the simulation of soil temperatures with thermal parameters estimated by heat transport inverse model was reasonably good (Table 5 and Fig.6). The RMSE of soil temperature at 5 cm soil depth (ranged from 2.0 to 4.2 °C) was large. The large errors might be caused by the insufficient contact of the soil temperature sensors at 5 cm soil depth. The RMSE of soil temperatures at 10–50 cm soil depth ranged from 1.0 to 2.5 °C with the MRE from 4.4% to 13% for the P1 treatment; the RMSE ranged from 1.1 to 2.5 °C with the MRE from 5.5% to 10.6% (except at 20 cm soil depth) for the P2 treatment; and the RMSE from 1.2 to 2.2 °C with the MRE from 4.5% to 12.7% for the P3 treatment. Unlike the simulations of soil water, the simulations of soil temperatures in all treatments were satisfactory. This result indicated that the spatial heterogeneity in thermal parameters in the field was less than in

Table 4
The root mean square errors (RMSE), mean absolute errors (MAE), and mean relative errors (MRE) between simulated and observed daily soil water contents for the P1, P2, and P3 treatments at different positions by simulation with parameters estimated with soil textural information (S1), soil water retention curve (S2), and Inverse model (S3).

Depth (cm)	Error	Treatment								
		P1			P2			P3		
		Top	Side	Base	Top	Side	Base	Top	Side	Base
S1										
0-10	RMSE (cm^3 cm^{-3})	0.072	0.034	0.043	0.028	0.024	0.030	0.074	0.048	0.037
	MAE (cm^3 cm^{-3})	0.064	0.025	0.038	0.022	0.019	0.023	0.064	0.042	0.031
	MRE (%)	51.8	15.3	25.3	11.8	9.4	9.2	51.1	25.1	15.7
10-20	RMSE (cm^3 cm^{-3})	0.031	0.028	0.055	0.034	0.028	0.039	0.037	0.020	0.024
	MAE (cm^3 cm^{-3})	0.026	0.024	0.052	0.028	0.019	0.033	0.030	0.017	0.021
	MRE (%)	12.6	14.0	36.7	13.0	8.0	19.9	17.1	7.1	11.1
20-30	RMSE (cm^3 cm^{-3})	0.037	0.052	0.058	0.038	0.028	0.022	0.019	0.017	0.016
	MAE (cm^3 cm^{-3})	0.033	0.049	0.055	0.034	0.024	0.017	0.017	0.014	0.015
	MRE (%)	19.3	33.7	40.3	13.3	10.2	7.2	6.9	7.2	7.3
30-50	RMSE (cm^3 cm^{-3})	0.041	0.052	0.021	0.016	0.023	0.018	0.025	0.035	0.077
	MAE (cm^3 cm^{-3})	0.038	0.050	0.019	0.014	0.020	0.018	0.025	0.035	0.077
	MRE (%)	24.5	34.7	8.9	7.1	11.3	8.0	12.9	19.0	26.0
S2										
0-10	RMSE (cm^3 cm^{-3})	0.110	0.072	0.081	0.065	0.061	0.038	0.117	0.095	0.066
	MAE (cm^3 cm^{-3})	0.100	0.063	0.072	0.060	0.055	0.032	0.107	0.091	0.052
	MRE (%)	78.5	35.7	47.1	31.3	27.7	14.5	82.0	52.1	28.5
10-20	RMSE (cm^3 cm^{-3})	0.058	0.072	0.073	0.059	0.048	0.068	0.086	0.051	0.069
	MAE (cm^3 cm^{-3})	0.048	0.065	0.065	0.050	0.044	0.058	0.079	0.045	0.063
	MRE (%)	24.7	37.4	45.5	25.0	20.7	35.1	42.7	20.3	32.9
20-30	RMSE (cm^3 cm^{-3})	0.072	0.072	0.061	0.028	0.025	0.021	0.047	0.065	0.054
	MAE (cm^3 cm^{-3})	0.063	0.063	0.056	0.024	0.021	0.017	0.042	0.059	0.049
	MRE (%)	37.5	43.2	40.9	10.1	9.2	7.5	18.7	29.8	24.7
30-50	RMSE (cm^3 cm^{-3})	0.017	0.035	0.009	0.019	0.021	0.018	0.061	0.068	0.047
	MAE (cm^3 cm^{-3})	0.013	0.034	0.008	0.014	0.017	0.017	0.055	0.065	0.044
	MRE (%)	8.5	23.2	3.6	7.5	9.2	7.6	29.1	36.1	14.8
S3										
0-10	RMSE (cm^3 cm^{-3})	0.033	0.039	0.044	0.038	0.049	0.031	0.033	0.025	0.038
	MAE (cm^3 cm^{-3})	0.026	0.034	0.040	0.034	0.045	0.023	0.027	0.020	0.032
	MRE (%)	21.6	15.8	26.2	16.2	20.1	9.5	20.8	9.7	16.1
10-20	RMSE (cm^3 cm^{-3})	0.052	0.031	0.057	0.034	0.025	0.039	0.030	0.020	0.022
	MAE (cm^3 cm^{-3})	0.046	0.028	0.055	0.027	0.017	0.032	0.024	0.017	0.020
	MRE (%)	19.3	16.1	38.5	11.2	6.9	19.7	11.5	6.9	10.4
20-30	RMSE (cm^3 cm^{-3})	0.041	0.056	0.061	0.031	0.025	0.022	0.019	0.016	0.015
	MAE (cm^3 cm^{-3})	0.037	0.054	0.058	0.028	0.022	0.016	0.016	0.014	0.014
	MRE (%)	21.9	36.8	42.4	10.9	9.2	7.0	6.9	6.9	7.0
30-50	RMSE (cm^3 cm^{-3})	0.046	0.056	0.021	0.017	0.025	0.017	0.027	0.035	0.078
	MAE (cm^3 cm^{-3})	0.043	0.053	0.018	0.015	0.022	0.017	0.026	0.035	0.077
	MRE (%)	27.5	37.2	8.7	8.1	12.1	7.4	13.5	19.1	26.1

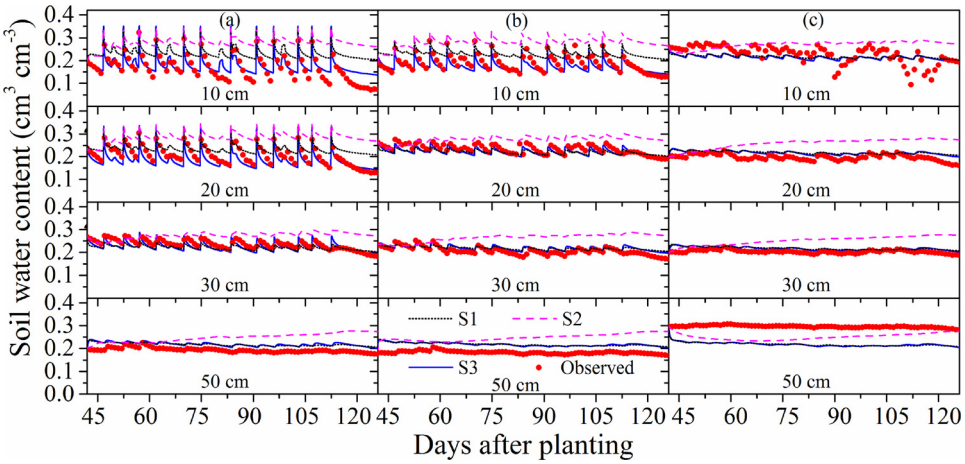

Fig. 5. Observed and simulated daily soil water content at different depths in (a) the top, (b) the side, and (c) the base of the bed for the P3 treatment with three simulation approaches: simulation with parameters estimated from soil textural information (S1), from experimentally measured soil water retention curve (S2), and from inverse modeling (S3).

soil hydraulic parameters. It was consistent with the report of Dahiya et al. (2007).

3.2. Soil water transport and distribution

Soil water distributions at the end of irrigation and during the following three days after the irrigation were simulated with the soil hydraulic parameters estimated by inverse modeling (Fig.7). The higher

Table 5
The root mean square errors (RMSE), mean absolute errors (MAE), and mean relative errors (MRE) between simulated and observed daily soil temperatures for the P1, P2, and P3 treatments at different positions.

Depth (cm)	Error	Treatment					
		P1		P2		P3	
		Top	Side	Top	Side	Top	Side
5	RMSE (°C)	2.7	4.2	3.9	3.3	2.0	4.2
	MAE (°C)	2.6	4.1	3.5	3.1	1.7	4.0
	MRE (%)	13.6	22.7	18.9	21.0	9.2	21.5
10	RMSE (°C)	1.1	2.5	2.5	2.1	1.2	1.5
	MAE (°C)	0.9	2.4	1.9	1.5	0.8	1.0
	MRE (%)	5.2	13.0	10.6	9.4	4.5	5.6
20	RMSE (°C)	1.2	1.1	4.0	2.1	1.5	1.6
	MAE (°C)	1.0	1.0	2.9	1.6	1.3	1.4
	MRE (%)	5.3	5.5	25.5	9.1	7.2	8.0
30	RMSE (°C)	1.2	1.3	1.7	1.5	1.9	1.5
	MAE (°C)	0.9	1.1	1.3	1.2	1.7	1.3
	MRE (%)	4.3	6.5	7.2	6.6	10.1	7.6
50	RMSE (°C)	1.4	1.0	1.9	1.1	2.2	2.2
	MAE (°C)	1.2	0.8	1.6	0.9	2.0	2.1
	MRE (%)	7.6	4.4	9.2	5.5	12.6	12.7

wetted soil percentage of drip irrigation led to a larger soil wetted zone. At the end of irrigation the depth of soil wetted front (soil water content equal to 0.22 $cm^3\ cm^{-3}$) was 24 cm for the P1 treatment, 27 cm for the P2 treatment, and 31 cm for the P3 treatment. The horizontal distance of the soil wetted front at 20 cm depth was 12 cm for the P1 treatment, 17 cm for the P2 treatment, and 23 cm for the P3 treatment. The larger difference of the soil wetted front in the horizontal direction meant that the high wetted soil percentage accelerated the horizontal soil water transport more than the vertical soil water transport.

After irrigation, the soil water content reduced rapidly at 0–20 cm soil depth during the first day because of the larger soil hydraulic conductivity at the raised bed. The smaller soil water content meant adequate aeration for potato tubers. It was one of the reasons why the raised bed could benefit potato growth (Harms and Konschuh, 2010). During the second and third days after irrigation, there was soil water downward transport for the P2 and P3 treatments but not for the P1 treatment. This meant that a higher wetted soil percentage could cause more deep percolation. The wetted soil percentage of 35% (P1) was enough for the potato growth in this area.

3.3. Soil temperature transport and distribution

The soil temperatures between the P1 and P3 treatments were similar, although the average soil temperature for the P1 treatment was 0.1-0.7 °C higher than for the P3 treatment (Fig.8). Li et al. (2017) also reported small soil temperature differences in different irrigation treatments. The soil temperature for the P2 treatment was the lowest among the three treatments. This result was reasonable as soil temperature could be affected not only by the soil moisture but also by the plant canopy. The potato plant canopy varied too much in the field: the lowest soil temperature for the P2 treatment might be caused by the larger canopy around the soil temperature sensors.

4. Summary and conclusion

In this study, HYDRUS-2D was used to simulate soil water and heat transport in a potato field under surface drip irrigation with raised beds and full plastic-film mulch. Three approaches were used to evaluate the soil water simulation with parameters derived from soil textural information (S1), from experimentally measured soil water retention curve (S2), and from inverse modeling (S3). All the three approaches performed unsatisfactorily for the P1 treatment and at 50 cm soil depth in the base of the bed for the P3 treatment because of the soil spatial heterogeneity. The performance of S2 was the worst for all treatments, giving a high RMSE ($> 0.05\ cm^3\ cm^{-3}$). The performance of S1 was much better than S2 with an RMSE ranged from 0.014 to 0.039 $cm^3\ cm^{-3}$ at 10–50 cm soil depth for the P2 treatment and from 0.016 to 0.048 $cm^3\ cm^{-3}$ at 20–50 cm soil depth (except at 50 cm soil depth in the base of the bed) for the P3 treatment. The performance of S3 was better than S1, especially at 0–10 cm soil depth. The RMSE of S3 for the P3 treatment ranged from 0.015 to 0.038 $cm^3\ cm^{-3}$ at 10–50 cm soil depth (except at 50 cm soil depth in the base of the bed). The soil temperature simulation with thermal parameters estimated by inverse model was satisfactory with the RMSE ranged from 1.0 to 2.5 °C at 10–50 cm soil depth (except at 20 cm soil depth for the P2 treatment).

The simulated soil water in the raised bed decreased quickly after irrigation, which could maintain adequate aeration for potato growth, irrespective of the wetted soil percentage. The downward transport of soil water still existed on the second and third days after irrigation for the P2 and P3 treatments. The soil temperatures between the P1 and P3 treatments were similar. The large soil temperature difference could be caused by plant canopy differences. Generally, a wetted soil percentage of 35% could provide suitable soil water and heat conditions under

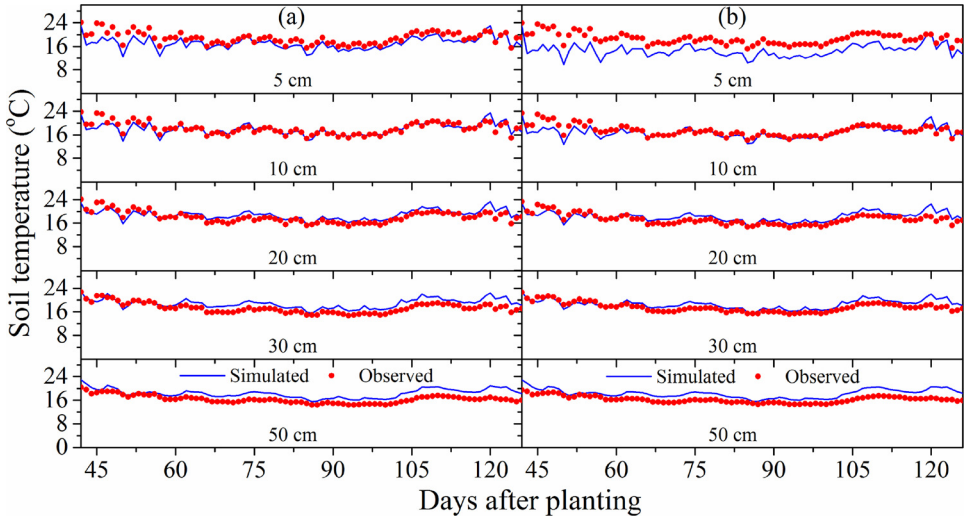

Fig. 6. Observed and simulated daily soil temperatures at different depths in (a) the top and (b) the side of the bed for the P3 treatment with simulation using parameters estimated from inverse modeling.

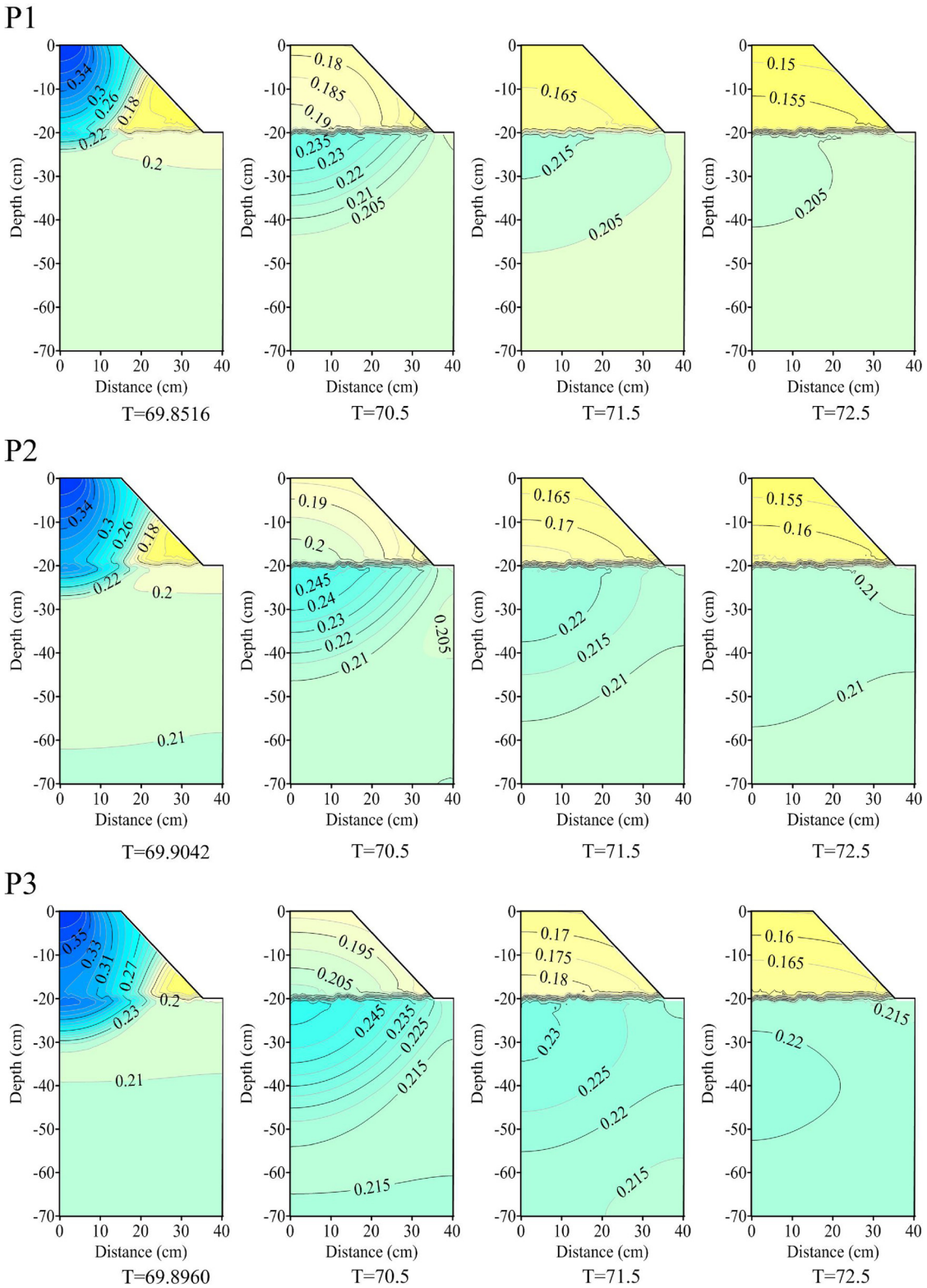

Fig. 7. Simulated soil water distributions at the end of irrigation (on 69.8516 days after planting for the P1 treatment, 69.9042 days for the P2 treatment, 69.8960 days for the P3 treatment) and the following three days after the irrigation (on 70.5 days, 71.5 days, and 72.5 days after planting) for the P1, P2, and P3 treatments.

surface drip irrigation with raised beds and full plastic-film mulch for potato growth in this area.

In conclusion, the HYDRUS-2D could be used to simulate soil water flow and heat transport in drip irrigated potato field with raised beds and full plastic-film mulch. Furthermore, the calibrated HYDRUS-2D was useful to derive the distribution of soil water and heat under different combination of emitter distance and discharge and irrigation scheduling for potato production.

Acknowledgements

The financial support of this study came from Program 201501017

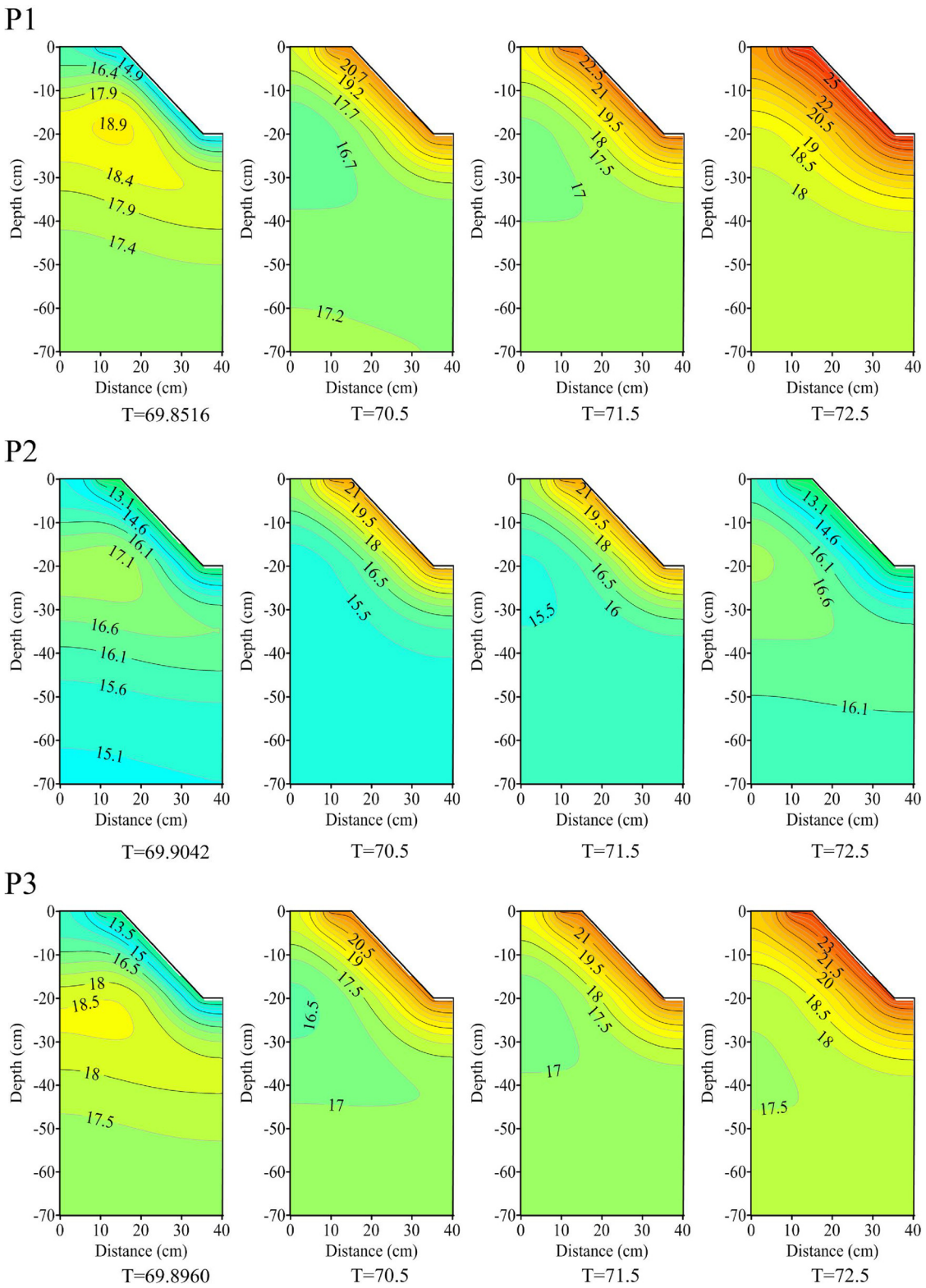

Fig. 8. Simulated soil temperature distributions at the end of irrigation (on 69.8516 days after planting for the P1 treatment, 69.9042 days for the P2 treatment, 69.8960 days for the P3 treatment) and the following three days after the irrigation (on 70.5 days, 71.5 days, and 72.5 days after planting) for the P1, P2, and P3 treatments.

of the Ministry of Water Resources of China and Program51579240 and 51439006 of National Natural Science Foundation of China. The first author studied the model in Lancaster University from April 2016 to October 2016 supported by China Scholarship Council (CSC), British Council (BC), and Newton Fund.

References

Ajdary, K., Singh, D.K., Singh, A.K., Khanna, M., 2007. Modelling of nitrogen leaching from experimental onion field under drip fertigation. Agric. Water Manage. 89, 15–28.
Allen, R.G., Pereira, L.S., Raes, D., Smith, M., 1998. Crop Evapotranspiration: Guidelines

for Computing Crop Water Requirements. FAO Irrigation and Drainage Paper No. 56. FAO, Rome, Italy.
Assouline, S., 2002. The effects of microdrip and conventional drip irrigation on water distribution and uptake. Soil Sci. Soc. Am. J. 66, 1630–1636.
Chen, L.J., Feng, Q., Li, F.R., Li, C.S., 2014. A bidirectional model for simulating soil water flow and salt transport under mulched drip irrigation with saline water. Agric. Water Manage. 146, 24–33.
Chung, S.O., Horton, R., 1987. Soil heat and water flow with a partial surface mulch. Water Resour. Res. 23 (12), 2175–2186.
Coelho, F.E., Or, D., 1997. Applicability of analytical solutions for flow from point sources to drip irrigation management. Soil Sci. Soc. Am. J. 61, 1331–1341.
Cook, F.J., Thorburn, P.J., Bristow, K.L., Cote, C.M., 2003. Infiltration from surface and buried point sources: the average wetting water content. Water Resour. Res. 39, 1364–1369.
Cropper, S.C., Perfect, E., van den Berg, E.H., Mayes, M.A., 2011. Comparison of average and point capillary pressure-saturation functions determined by steady-state centrifugation. Soil Sci. Soc. Am. J. 75 (1), 17–25.
Dahiya, R., Ingwersen, J., Streck, T., 2007. The effect of mulching and tillage on the water and temperature regimes of a loess soil: experimental findings and modeling. Soil Till. Res. 96, 52–63.
Darwish, T., Atallah, T., Hajhasan, M., Chranek, S., 2003. Management of nitrogen by fertigation of potato in Lebanon. Nutr. Cycl. Agroecosys. 67, 1–11.
de Vries, D.A., 1963. In: van Wijk, R.W. (Ed.), The Thermal Properties of Soils, In Physics of Plant Environment. North Holland, Amsterdam, pp. 210–235.
Feddes, R.A., Kowalik, P.J., Zaradny, H., 1978. Simulation of Field Water Use and Crop Yield. John Wiley and Sons, New York, NY.
Gärdenäs, A.I., Hopmans, J.W., Hanson, B.R., Šimůnek, J., 2005. Two-dimensional modeling of nitrate leaching for various fertigation scenarios under micro-irrigation. Agric. Water Manage. 74, 219–242.
Hanson, B.R., Šimůnek, J., Hopmans, J.W., 2006. Evaluation of urea–ammonium–nitrate fertigation with drip irrigation using numerical modeling. Agric. Water Manage. 86, 102–113.
Harms, T.E., Konschuh, M.N., 2010. Water savings in irrigated potato production by varying hill-furrow or bed-furrow configuration. Agric. Water Manage. 97, 1399–1404.
Holt, N., Shukla, S., Hochmuth, G., Muñoz-Carpena, R., Ozores-Hampton, M., 2017. Transforming the food-water-energy-land-economic nexus of plasticulture production through compact bed geometries. Adv. Water Resour. 110, 515–527.
Hopmans, J.W., Šimunek, J., Bristow, K.L., 2002. Indirect estimation of soil thermal properties and water flux using heat pulse probe measurements: geometry and dispersion effects. Water Resour. Res. 38 (1) 7, 1-7, 14.
Keller, J., Karmeli, D., 1974. Trickle irrigation design parameters. Trans. ASAE 17, 678–684.
Li, X.W., Jin, M.G., Huang, J.O., Yuan, J.J., 2015a. The soil-water flow system beneath a cotton field in arid north-west China, serviced by mulched drip irrigation using brackish water. Hydrogeol. J. 23, 35–46.
Li, X.Y., Shi, H.B., Šimůnek, J., Gong, X.W., Peng, Z.Y., 2015b. Modeling soil water dynamics in a drip-irrigated intercropping field under plastic mulch. Irrig. Sci. 33 (4), 289–302.
Li, X.Y., Šimůnek, J., Shi, H.B., Yan, J.W., Peng, Z.Y., Gong, X.W., 2017. Spatial distribution of soil water, soil temperature, and plant roots in a drip-irrigated intercropping field with plastic mulch. Eur. J. Agron. 83, 47–56.
Liakatas, A., Clark, J.A., Monteith, J.L., 1986. Measurements of the heat balance under plastic mulches. Part I. Radiation balance and soil heat flux. Agric. For. Meteorol. 36, 223–227.
Liu, M.X., Yang, J.S., Li, X.M., Yu, M., Wang, J., 2013. Numerical simulation of soil water dynamics in a drip irrigated cotton field under plastic mulch. Pedosphere 23 (5), 620–635.
Mortensen, A.P., Hopmans, J.W., Mori, Y., Šimůnek, J., 2006. Multi-functional heat pulse probe measurements of coupled vadose zone flow and transport. Adv. Water Resour. 29, 250–267.
Mualem, Y., 1976. A new model for predicting the hydraulic conductivity of unsaturated porous media. Water Resour. Res. 12 (3), 513–522.
Nakhaei, M., Šimůnek, J., 2014. Parameter estimation of soil hydraulic and thermal property functions for unsaturated porous media using the HYDRUS-2D code. J. Hydrol. Hydromech. 62 (1), 7–15.
Patel, N., Rajput, T.B.S., 2008. Dynamics and modeling of soil water under subsurface drip irrigated onion. Agric. Water Manage. 95, 1335–1349.
Phogat, V., Mahadevan, M., Skewes, M., Cox, J.W., 2012. Modelling soil water and salt dynamics under pulsed and continuous surface drip irrigation of almond and implications of system design. Irrig. Sci. 30, 315–333.
Phogat, V., Skewes, M.A., Cox, J.W., Sanderson, G., Alam, J., Šimůnek, J., 2014. Seasonal simulation of water, salinity and nitrate dynamics under drip irrigated mandarin (*Citrus reticulata*) and assessing management options for drainage and nitrate leaching. J. Hydrol. 513, 504–516.
Qi, Z.J., Feng, H., Zhao, Y., Zhang, T.B., Yang, A.Z., Zhang, Z.X., 2018. Spatial distribution and simulation of soil moisture and salinity under mulched drip irrigation combined with tillage in an arid saline irrigation district, northwest China. Agric. Water Manage. 201, 219–231.
Reatto, A., Da Silva, E.M., Bruand, A., Martins, E.S., Lima, J.E.F.W., 2008. Validity of the centrifuge method for determining the water retention properties of tropical soils. Soil Sci. Soc. Am. J. 72 (6), 1547–1553.
Ryżak, M., Bieganowski, A., 2011. Methodological aspects of determining soil particle-size distribution using the laser diffraction method. J. Plant Nutr. Soil Sci. 174, 624–633.
Schaap, M.G., Leij, F.J., van Genuchten, M.T., 2001. Rosetta: a computer program for estimating soil hydraulic parameters with hierarchical pedotransfer functions. J. Hydrol. 251, 163–176.
Shock, C.C., Pereira, A.B., Eldredge, E.P., 2007. Irrigation best management practices for potato. Am. J. Potato Res. 84, 29–37.
Šimůnek, J., Genuchten, M.T., 1996. Estimating unsaturated soil hydraulic properties from tension disc infiltrometer data by numerical inversion. Water Resour. Res. 32 (9), 2683–2696.
Šimůnek, J., Nimmo, J.R., 2005. Estimating soil hydraulic parameters from transient flow experiments in a centrifuge using parameter optimization technique. Water Resour. Res. 41, W04015.
Šimůnek, J., Suarez, D.L., 1993. UNSATCHEM-2D Code for Simulating Two-dimensional Variably Saturated Water Flow, Heat Transport, Carbon Dioxide Production and Transport, and Multicomponent Solute Transport With Major Ion Equilibrium and Kinetic Chemistry, Version 1.1, Research Report No. 128. U.S. Salinity Laboratory, USDA, ARS, Riverside, CA.
Šimůnek, J., van Genuchten, M.T., Šejna, M., 2008. Development and applications of the HYDRUS and STANMOD software packages and related codes. Vadose Zone J. 7 (2), 587–600.
Šimůnek, J., van Genuchten, M.T., Šejna, M., 2016. Recent developments and applications of the HYDRUS computer software packages. Vadose Zone J. 15 (7), 25.
Sophocleous, M., 1979. Analysis of water and heat flow in unsaturated-saturated porous media. Water Resour. Res. 15 (5), 1195–1206.
Subbaiah, R., 2013. A review of models for predicting soil water dynamics during trickle irrigation. Irrig. Sci. 31, 225–258.
Tiwari, K.N., Singh, A., Mal, P.K., 2003. Effect of drip irrigation on yield of cabbage (*Brassica oleracea* L. Var. *capitata*) under mulch and non-mulch conditions. Agric. Water Manage. 58, 19–28.
Van Dam, J., Kooman, P.L., Struik, P.C., 1996. Effects of temperature and photoperiod on early growth and final number of tubers in potato (*Solanum tuberosum* L.). Potato Res. 39, 51–62.
Van den Berg, E.H., Perfect, E., Tu, C., Knappett, P.S.K., Leao, T.P., Donat, R.W., 2009. Unsaturated hydraulic conductivity measurements with centrifuges: a review. Vadose Zone J. 8 (3), 531–547.
van Genuchten, M.T., 1980. A closed-form equation for predicting the hydraulic conductivity of unsaturated soils. Soil Sci. Soc. Am. J. 44, 892–898.
van Genuchten, M.T., Leij, F.J., Yates, S.R., 1991. The RETC Code for Quantifying the Hydraulic Functions of Unsaturated Soils, Version 1.0. EPA Report 600/2-91/065. U.S. Salinity Laboratory, USDA, ARS, Riverside, California.
Vrugt, J.A., Hopmans, J.W., Šimůnek, J., 2001a. Calibration of a two-dimensional root water uptake model. Soil Sci. Soc. Am. J. 65 (4), 1027–1037.
Vrugt, J.A., van Wijk, M.T., Hopmans, J.W., Šimůnek, J., 2001b. One-, two-, and three-dimensional root water uptake functions for transient modeling. Water Resour. Res. 37 (10), 2457–2470.
Wang, F.X., Kang, Y.H., Liu, S.P., Hou, X.Y., 2007. Effects of soil matric potential on potato growth under drip irrigation in the North China Plain. Agric. Water Manage. 88, 34–42.
Wang, F.X., Wu, X.X., Shock, C.C., Chu, L.Y., Gu, X.X., Xue, X., 2011. Effects of drip irrigation regimes on potato tuber yield and quality under plastic mulch in arid Northwestern China. Field Crops Res. 122, 78–84.
Wang, Z.M., Jin, M.G., Šimůnek, J., van Genuchten, M.T., 2014. Evaluation of mulched drip irrigation for cotton in arid Northwest China. Irrig. Sci. 32, 15–27.
Yaghi, T., Arslan, A., Naoum, F., 2013. Cucumber (*Cucumis sativus*, L.) water use efficiency (WUE) under plastic mulch and drip irrigation. Agric. Water Manage. 128, 149–157.
Zhang, Y.L., Wang, F.X., Shock, C.C., Yang, K.J., Kang, S.Z., Qin, J.T., Li, S.E., 2017a. Effects of plastic mulch on the radiative and thermal conditions and potato growth under drip irrigation in arid Northwest China. Soil Till. Res. 172, 1–11.
Zhang, Y.L., Wang, F.X., Shock, C.C., Yang, K.J., Kang, S.Z., Qin, J.T., Li, S.E., 2017b. Influence of different plastic film mulches and wetted soil percentages on potato grown under drip irrigation. Agric. Water Manage. 180, 160–171.
Zhao, Y., Peth, S., Horn, R., Krümmelbein, J., Ketzer, B., Gao, Y.Z., Doerner, J., Bernhofer, C., Peng, X.H., 2010. Modeling grazing effects on coupled water and heat fluxes in Inner Mongolia grassland. Soil Till. Res. 109, 75–86.
Zhao, H., Wang, R.Y., Ma, B.L., Xiong, Y.C., Qiang, S.C., Wang, C.L., A, L.C., Li, F.M., 2014. Ridge-furrow with full plastic film mulching improves water use efficiency and tuber yields of potato in a semiarid rainfed ecosystem. Field Crops Res. 161, 137–148.
Zhao, Y., Zhai, X.F., Wang, Z.H., Li, H.J., Jiang, R., Hill, R.L., Si, B., Feng, H., 2018. Simulation of soil water and heat flow in ridge cultivation with plastic film mulching system on the Chinese Loess Plateau. Agric. Water Manage. 202, 99–112.
Zur, B., 1996. Wetted soil volume as a design objective in trickle irrigation. Irrig. Sci. 16, 101–105.